ARTICLE

Terahertz spectroscopy and imaging of potential phantoms with defect classification

Keana Rylie E. Pasoquen[1], Vincent Gene L. Otero[1], Rovie S. de Ramos[1], Mary Alyssa Benilde H. Aringay[1], Prince Ranier C. Rana[1], Gellin M. Gonzales[1], Jonathan S. Morada[1], Denzel Jeremiah B. Mulato[1], Arvin Lester C. Jusi*[1], Arnel A. Salvador[2], Elmer S. Estacio[2], and Alvin Karlo G. Tapia[1]

[1]Institute of Physics, University of the Philippines Los Baños, Laguna, 4031, Philippines
[2]National Institute of Physics, University of the Philippines Diliman, Quezon City, 1101, Philippines

ABSTRACT

Terahertz (THz) spectroscopy and imaging were used for probing defects in potential imaging phantoms. Imaging phantoms are materials that can be used to mimic biological systems or general industrial materials. Polyvinyl acetate, silicone and plaster of Paris were used to simulate thin, gel-like, and solid systems, respectively. Defects and impurities were introduced for each material. The THz properties and images of the samples were determined using THz time-domain spectroscopy (THz-TDS). The THz absorption spectra and images were able to reveal variations between the control samples and samples with defects. This clearly shows that these variations are correlated with the defects introduced into the material. These results demonstrate the effectiveness of THz-TDS and imaging in detecting defects even across a wide variety of materials. Furthermore, using principal component analysis (PCA) of the THz images, it was observed that the THz properties varied depending on the type of defect introduced into the samples. PCA results showed distinct clusters for different defects and impurities in the samples. These results highlight a promising non-destructive method for identifying material defects, which can complement other non-destructive evaluation methods, ensuring the quality and safety of materials and products across various industries.

*Corresponding author
Email Address: acjusi@up.edu.ph
Date received: 28 January 2025
Dates revised: 29 April 2025
Date accepted: 01 June 2025
DOI: https://doi.org/10.54645/2025181QIS-68

INTRODUCTION

In the industrial setting, several processes greatly rely on how well the properties and composition of materials are known. However, detection of defects or impurities in materials presents a challenge as defects widely vary in type, size, and location in the material. Spectroscopy offers a promising solution to this problem, as studies suggest that the spectroscopic properties of materials are dependent on the defects or impurities present in a material (Antony et al. 2021). Still, spectroscopic techniques can sometimes be highly specialized and the wide variation of defects in the industrial setting cannot be catered unless multiple spectroscopic techniques are employed. Such an approach can be costly and time-consuming because spectroscopic systems are often expensive, and one will be required to perform a number of measurements for a single material. Therefore, the remaining challenge is to find a spectroscopic technique that can readily identify a wide variety of defects, making the identification process cheaper and more time-efficient.

One promising spectroscopic technique is the use of terahertz (THz) radiation, a type of electromagnetic radiation whose frequency lies between the infrared and the microwave regions, in analyzing diverse types of samples due to its high-resolution

KEYWORDS

terahertz spectroscopic imaging; imaging phantoms; principal component analysis

imaging capabilities (Rostami et al. 2010). It has a unique characteristic of being strongly absorbed by materials with large electrical conductivity or large static dipoles like water (Mittleman 2018). Its advantage over other spectroscopic techniques is that THz radiation has a low penetration depth and is non-ionizing in nature, making it safe for imaging applications involving biological samples and dielectric materials. This also makes THz radiation an attractive option for repeated imaging procedures and longitudinal studies (Konnikova et al. 2021). Moreover, it can provide polarization-resolved measurements, which translates to a high image contrast.

Another advantage of THz spectroscopy is its ability to identify a wide variety of materials, ranging from inorganic particles to organic compounds, regardless of their chemical composition. This versatility makes THz spectroscopic measurements and imaging an effective method for detection of defects or impurities (Sasaki et al. 2018). In a 2008 study, Jördens, C. and Koch, M., used pulsed THz imaging in order to identify the presence of foreign bodies such as stones, nuts, microplastics, and glass embedded in chocolate. Although the information obtained from the intensity image required necessary image processing techniques to reduce false-alarm rate detection, the study was able to distinguish foreign bodies and wanted ingredients like nuts by analyzing the shape of the temporal waveform. This highlights the method's sensitivity to detecting a broad spectrum of impurities, including both solid and particulate materials. Adding proof to the versatility of THz, a recent study by Shen et al. in 2021 reported that impurities in the form of weed, husk, wheat leaf, grain, and ladybugs present in wheat can be detected via the application of convolutional neural network (CNN) in THz imaging. In the same year, Hu, J. et al. successfully distinguished foreign bodies in milk powders with 100% recognition accuracy by implementing the random forest discrimination method in THz spectroscopy. In 2023, they extended their study using THz time-domain spectroscopy applied with different algorithms in the detection of exogenous and endogenous foreign bodies in fish (Hu et al. 2023). Furthermore, THz technology has an impurity detection application in both foods and biological samples. In the midst of the progressing development of THz technology in 2011, Kemp, M. argued that, despite its application for substance detection, this particular technology has several shortcomings (Kemp 2011). Aside from environmental factors that can cause THz spectral distortion, the composition of the sample itself can also contribute to the limitation of this technology. For instance, it is possible to detect misleading absorption frequency data that is not inherent to a neutral sample when observing reflected THz pulses (Trofimov et al. 2017). Nevertheless, the technology's ability to detect and identify impurities plays an important role in ensuring the safety and quality of a wide range of products, from food to pharmaceuticals, underscoring its crucial contribution to public health and safety.

The application of THz spectroscopy and imaging extends to the medical fields particularly in clinical diagnostics and quality assurance owing to its non-invasive and non-ionizing nature. The ability of THz spectroscopy to analyze the composition of biological tissues has been recently explored through the use of phantoms. Phantoms are physical models that mimic biological tissues with regard to their certain selected features in medical imaging and therapy (Wegner et al. 2023). Thus, these materials provide researchers with an adequate test environment, which helps lessen the risk of human subjects and animal testing. In 2022, a study on the THz characterization of polyvinyl alcohol-based hydrogel phantom has shown that its frequency-dependent properties are similar to human skin and have indicated its potential to be used as a human skin equivalent (Jayasanka et al. 2022). Furthermore, the application of phantoms in THz imaging has also enabled researchers to develop image-contrasting techniques to distinguish cancerous tissues from healthy tissues. A phantom study on carbon-based nanoparticles as a contrast agent for breast cancer has shown that onion-like carbon has a promising property as a THz contrast agent when it was implemented into a breast tumor phantom (Bowman et al. 2017).

To take advantage of the suitability of THz spectroscopy and imaging in studying phantoms, this study used THz Time-Domain Spectroscopy (THz-TDS) and imaging to observe the properties of three materials—polyvinyl acetate (PVA), silicone, and plaster of Paris (PoP)—which are selected as phantom mimics of thin tissues, soft tissues, and hard tissues. Defects were introduced into the samples which were created based on mechanical or structural defects and the presence of foreign materials, among others. For example, PoP has the potential to mimic hard tissues like bones. The silicone samples can mimic softer tissues and the PVA samples can mimic thin tissues like skin. After introducing the defect into the samples, defect classification was done by integrating classification algorithms, such as Principal Component Analysis (PCA), to the results of the THz measurements.

MATERIALS AND METHOD

THz Spectroscopy and Imaging

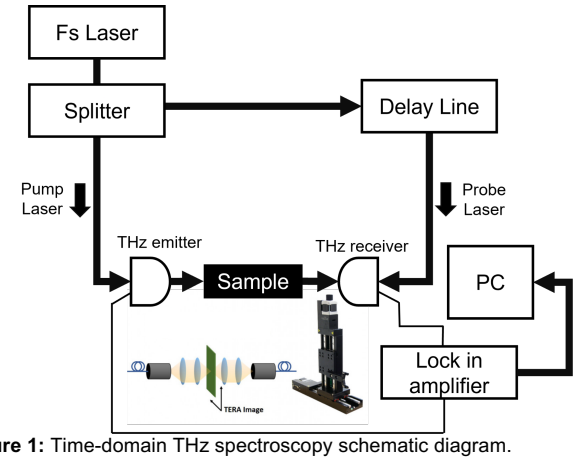

Figure 1: Time-domain THz spectroscopy schematic diagram.

A schematic of the THz time-domain spectroscopy system can be seen in figure 1. Measurements in THz-TDS yield amplitude and phase information which can be used to directly calculate the index of refraction and the absorption coefficient of the sample in the THz range. The time-domain signals from the reference and from the sample are transformed into the frequency domain through Fourier transformation.

A THz spectrometer from Menlo Systems (Martinsried, Germany) was used to investigate the THz properties of the samples. The samples were placed on the sample holder attached on the movable arm, which can be adjusted by specifying the desired X and Y coordinates. These coordinates simply limit the region within the material, which will be measured by the spectrometer. For all measurements, it was made certain that the THz detector was able to cover the 10 mm diameter region of the sample holder which contains the samples. The THz image of each sample, as well as its spectral information, was obtained through the continuous scanning of the spectrometer. The scanning rate of the system is 16 Hz (16 THz pulses per second). The scanning rate and measurement time varies per sample due to differences in hydration properties of the materials. The measurement time for the samples ranged from five to ten minutes.

To facilitate uniformity during data gathering, the following parameters were maintained all throughout the image acquisition process. Step size was set to 0.25 mm for both the X and Y coordinates of all images to ensure better resolution quality. The environmental parameters such as temperature and humidity were maintained from 20 - 21°C and 35 - 40%, respectively. For the sample thickness, the optimum thickness was chosen for each sample, such that the composition of the material was not compromised during image acquisition.

Sample Preparation

The study investigated the defects among three different potential phantoms which are polyvinyl acetate (PVA), silicone, and plaster of paris (PoP). The added defects for each phantom were also selected to introduce possible contrasting agents in the THz absorption of the samples. After sample preparation, each material was placed in the sample holder with an aperture diameter of 10 mm for image acquisition.

Polyvinyl Acetate (PVA)

Thin film samples having a thickness of approximately 0.9 mm were prepared by molding commercial polyvinyl acetate (PVA). PVA is a colorless generally nontoxic thermoplastic adhesive prepared through the polymerization of vinyl acetate. It is a widely used water-dispersed adhesive with its applications ranging from the manufacturing of glass fiber-reinforced plastics, production of automobile accessories, developments in the construction industry, and a lot more (Riedl 2015). Once PVA undergoes hydrolysis, it produces polyvinyl alcohol, which is also perceived as a skin and soft tissue phantom for a wide group of magnetic resonance techniques including optical tomography, or x-ray examination. Its outstanding similarity with human skin has even led to using PVA as a skin model for designing a computer game controller (Dabrowska et al. 2016). Three samples were prepared for this material: a control sample, a sample with a bubble defect, and a sample with an embedded silica gel (see figure 2). The first sample, or the control sample, consists of only pure PVA without any added defect. Each of the remaining samples consists of the PVA sample with defects which were intentionally added during the molding process. Bubble defects were added to the second sample and silica gel was embedded into the third sample. To facilitate drying, all the samples were left exposed to ambient air for approximately two hours. The samples were then tested when it became free-standing and mechanically robust.

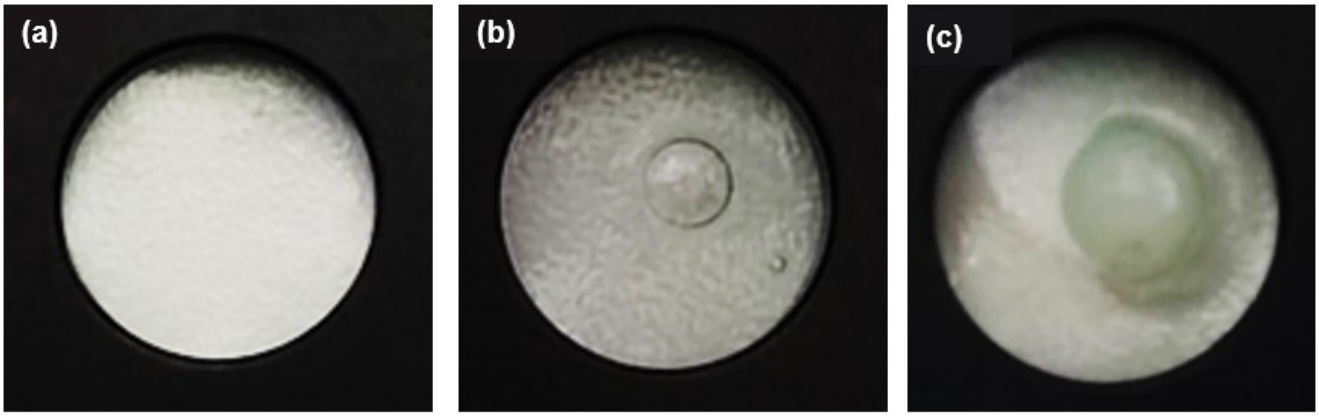

Figure 2: PVA samples: (a) Control sample, (b) PVA with a bubble defect, (c) PVA with the silica gel defect. The images were taken while each sample was loaded in the sample holder, the visible portion of each sample has a diameter of 10 mm.

Silicone

Silicones are synthetic polymers containing a repeating Si − O backbone and organic groups attached directly to the silicon atom through silicon-carbon bonds (LeVier et al. 1995). Silicone polymers are used in a variety of biomedical applications and industrial uses (Brook 2012). This material has also been studied to mimic properties of soft tissues for needle-based medical procedures. Wang et al. in their study have shown that a 40 wt% concentration of mineral oil with silicone provides the most similarity with soft tissues in terms of the elastic modulus and needle insertion force of the phantom (Wang et al. 2014).

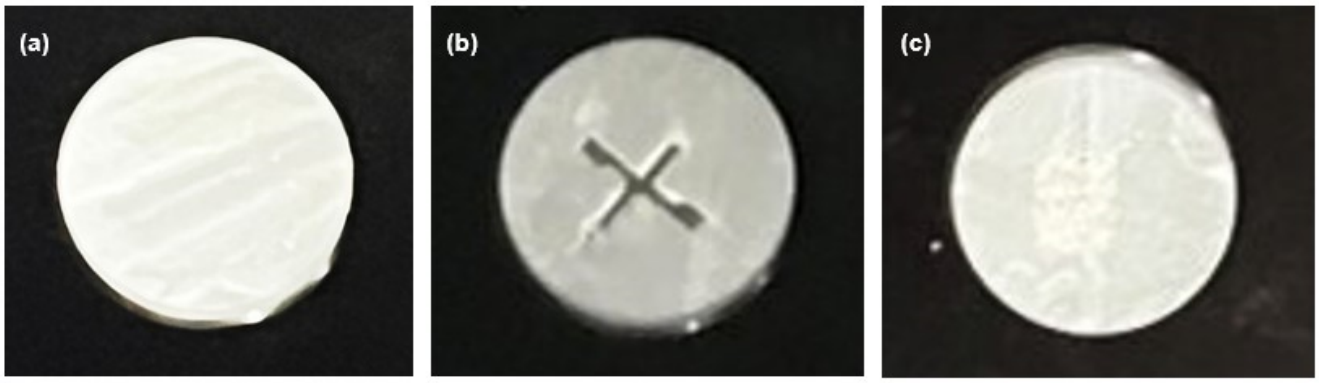

Figure 3: Silicone samples:(a) Control sample, (b) Sample with cross-shaped cut, (c) Sample with sponge. The images were taken while each sample was loaded in the sample holder, the visible portion of each sample has a diameter of 10 mm.

In this stage of the sample preparation, the silicone samples were developed using a silicone-based sealant and were fabricated using two sliding glasses compressed together to produce a thickness of 1.4 mm. The samples were cured for 48 hours before removing them from the mold. Using this technique, three silicone-based products were developed with different

defects. In figure 3, the first image illustrates the sample without any defects, which stands as the control sample, while the other two images show the samples with two different defects with a cut and a sponge, respectively. The cut sample was produced by inducing a cross-shaped cut on a silicone sample, while the sponge defect was produced by embedding a dish-washing sponge in the sample during the curing stage.

Plaster of Paris (PoP)

The composition of PoP is derived from calcium sulfate dihydrate, also referred to as gypsum, which is a naturally occurring rock-like substance found in rock salts. Once gypsum is heated to a certain temperature, it results in a powdery substance, which is commonly known as PoP (Colditz 2002). The use of PoP in this study was mainly to mimic properties of hard tissues, which are tissues with high degrees of hardness, usually located in bones or teeth. A recent development and validation of a low-cost pediatric pelvis phantom made use of PoP as the tissue equivalent material representing pediatric bone. Their results have shown that their fabricated phantom has a potential in dose and image quality optimization studies since it has provided suitable anatomical characteristics for X-ray imaging (Ali et al. 2018).

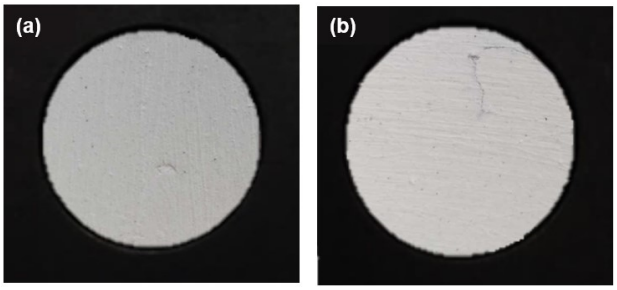

Figure 4: PoP samples: (a) Control sample and (b) Sample with aluminum defect. The images were taken while each sample was loaded in the sample holder, the visible portion of each sample has a diameter of 10 mm.

Five samples were made by mixing 10g of PoP with 5mL of water to keep the 2:1 ratio observed in the literature (see figure 4). Samples were then mixed with defects with one being mixed with pieces of aluminum foil, one with shredded PET, one with shaved styrofoam, and one sample was left unmixed but a scratch was placed on it to serve as both the control sample and the sample with the scratch defect as shown in figure 4. Samples were then left to air dry until solid and sanded down to the appropriate thickness for THz imaging which is about 1-2 mm.

DATA PROCESSING

THz Image Data Point Extraction

A generated THz image is described by an amplitude color gradient bar, wherein the value of the gradient corresponds to the THz waves transmitted through the sample. THz imaging was performed at an optimal step size that ensures efficient scanning time while maintaining high image resolution and minimizing the effects of moisture absorption for each sample. Depending on the amplitude of the THz radiation transmitted, the color of the pixel will be determined: for instance, blue for the low transmission and red for high transmission. Each pixel in the THz image corresponds to a THz time-domain spectrum. For each image, 15 data points are obtained. The image points from the defected samples were selected using the THz gradient amplitude of the control samples as a reference. Specifically, image points were chosen based on regions in the defected samples that exhibited variations in contrast compared to the control samples. Regions with amplitude values identical to those of the control samples were excluded from the selection. From the obtained images, the apparent defects appeared to have a different contrast to the THz images. The THz spectra were calculated from points within the selected region and were then compared with other defects and controls.

The THz absorption coefficient spectra were calculated from various points in the image as shown in figure 5. The significant fluctuations around 1.1 - 1.2 THz can be caused by the numerical errors from subtracting the reference spectra which are attributed to the THz absorption of water. Due to the strong absorption of water in the THz band, the characteristics of the environmental condition can affect the resulting spectra. Depending on the air pressure, the THz absorption spectra of air can range from 0.55 to 1.4 THz (Yang et al. 2021). The corresponding absorption coefficient of the point from the defects and the control were analyzed using principal component analysis (PCA).

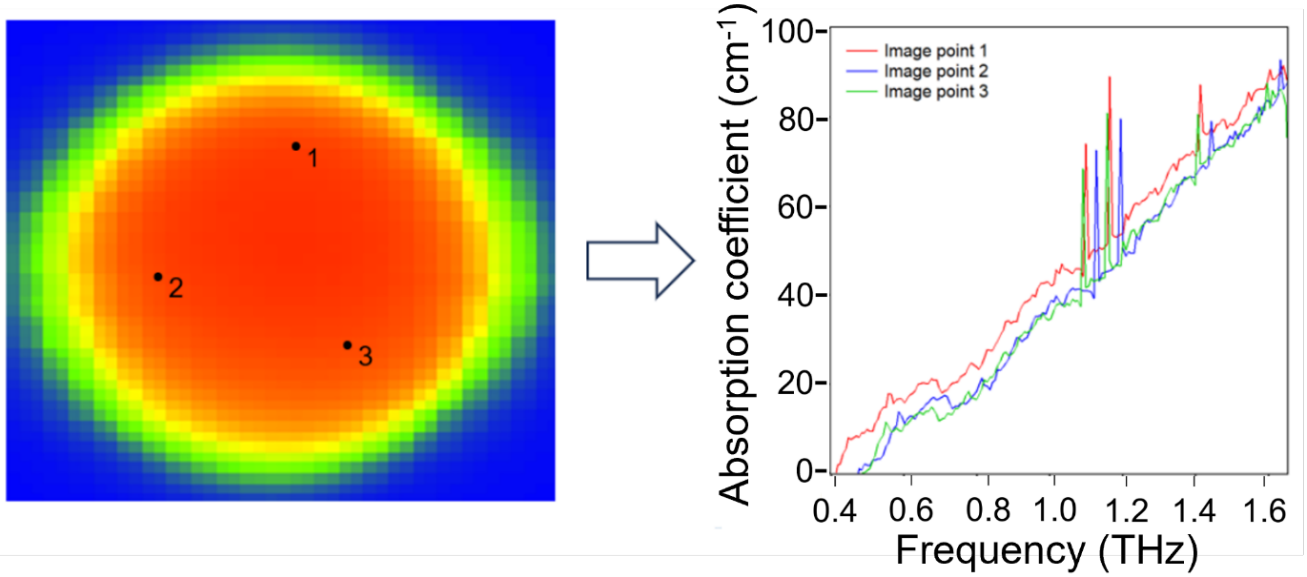

Figure 5: Sample THz absorbance spectra. The data shown in the spectra are from the first three data points of the control thin film sample.

Spectral Data to its Principal Components and Data Analysis

The spectral data obtained from the THz measurements cover the frequency ranging from 0.007 to 1.5 THz with an interval of approximately 0.01 THz. As an illustration, all the spectral data of the PVA samples are shown in figure 6. Commonly, comparing the spectral results of the samples requires considering each frequency value shown around 200 variables or dimensions. In this case, PCA acts as a dimension reduction analysis method to transform a data from higher to a much lower dimensional space (Jolliffe et al. 2016). In this study, 200 variables were transformed into principal components.

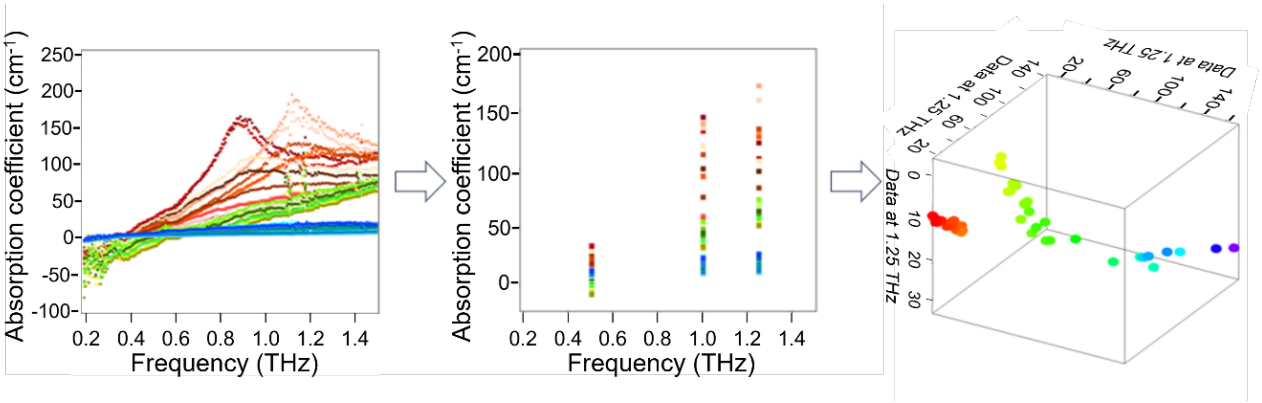

Figure 6: Calculation process from spectral data to principal components. For demonstration, three frequencies were selected among the frequency range of 0.007 - 1.5 THz. The principal components are calculated depending on the variance of the data set along the three frequencies. The resulting principal components serve as the axes in the PCA plot.

PCA is used to provide additional information when the scores are plotted using its principal components. In this study, two principal components are used for the corresponding score plots. The first and second principal components used in the analysis are labeled as PC1 and PC2, respectively. PC1 is the linear combination which accounts for the highest variance of the data set, whereas PC2 describes the linear combination for the next highest variance. The information contained in a certain data set can be summarized as a function of these linear combinations. Through this technique, one can transform an original data set into a new coordinate system which is structured by the principal components.

In the score plot, the formation of clusters in the PCA models can provide relevant information, such as the composition of the sample (El Haddad et al. 2013). Moreover, a study by Xie et al. (2018) reported that big data applications for the THz spectrum are attracting several areas of research as they contain a large quantity of data with a highly diverse data category. It was also mentioned that PCA, when compared to primitive data analysis, is more advantageous in determining differences and relationships between the internal variables of the material. A recent study by Wang et al. (2017) reported that due to the different responses of different rocks in the THz radiation, they could be distinguished by employing a mathematical method. It was indicated that PCA has successfully classified different materials when employed in THz-TDS. In 2015, Jiang, et al. reported that when PCA was performed with their normal, slightly moldy, moderately moldy, and seriously moldy wheat samples, the resulting principal components were able to cluster the different mold states (Jiang et al. 2015).

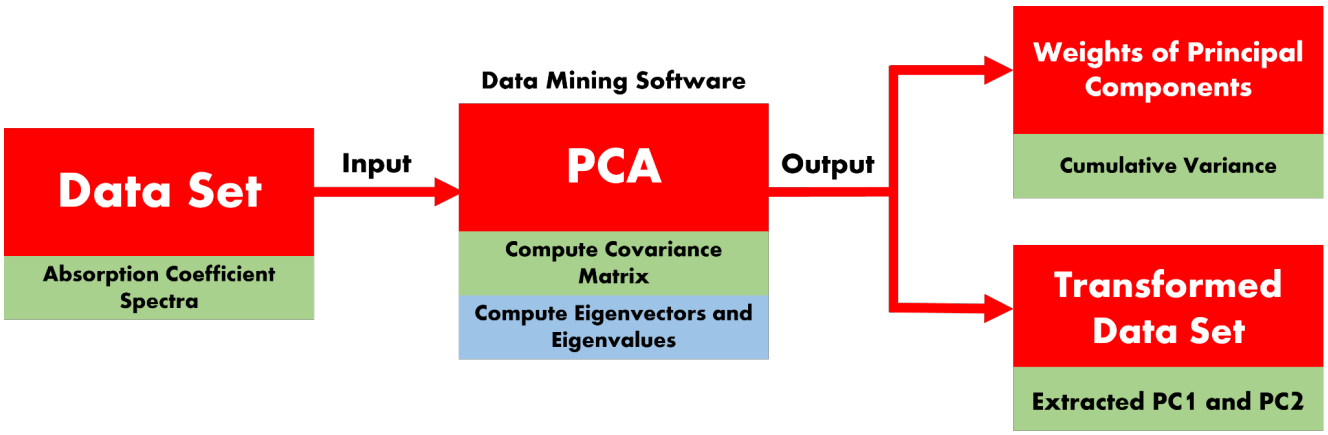

Figure 7: Modeling PCA in the data mining software

The process used in PCA modeling is shown in Figure 7. The data set used in modeling the PCA comes from the absorption coefficient spectra of the samples. This serves as the input for the data mining software, which normalizes the dataset and automatically computes the covariance and correlation matrix together with its eigenvector and eigenvalues. The calculated eigenvector will be used as the new feature vector in the transformed data space where the principal components serve as the axes. In selecting the appropriate number of principal components for the score plot, the number of components was chosen with a cumulative variance of at least 80%. Thus, the cumulative variance of the PC1 and PC2 of all the samples was sufficient to describe the data and were therefore used to graph the score plot.

RESULTS AND DISCUSSION

THz Images

The THz image reflects the transmission of the wave at each point. The transmission amplitude is represented in the gradient bar values. Each pixel from the THz image corresponds to a value in the gradient bar, which indicates the amplitude of the THz signal that was measured by the detector at that point.

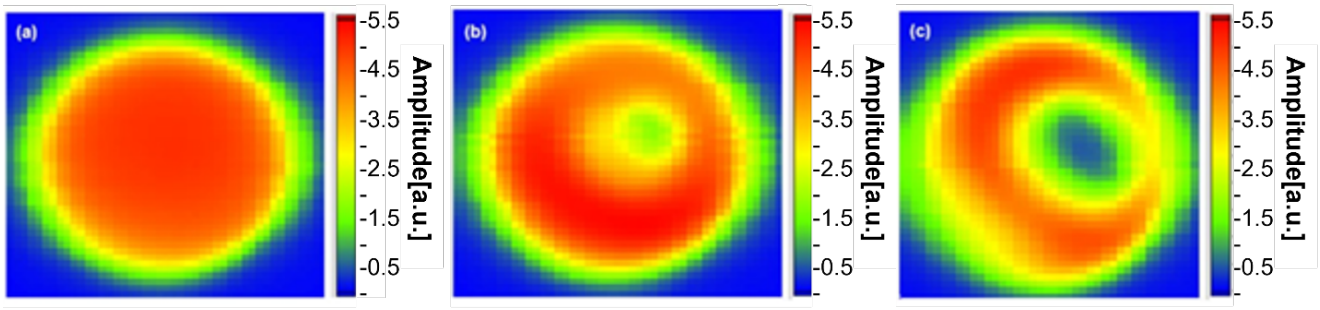

Figure 8: THz absorbance images of the PVA samples: (a) Control sample, (b) PVA with bubble defect, (c) PVA with silica gel defect

Bubble defects and silica gel defects were successfully induced in the PVA samples. The THz images of the PVA samples with defects showed clear variations from the control as illustrated in figure 8. While the control sample showed a constant THz transmission across its surface, with the maximum THz gradient amplitude at 5.5 as seen in figure 8a, the samples with defects exhibited higher THz absorption in the regions of the defects as seen in figures 8b and 8c. This shows agreement with the aforementioned potential of THz imaging in characterizing defects in samples.

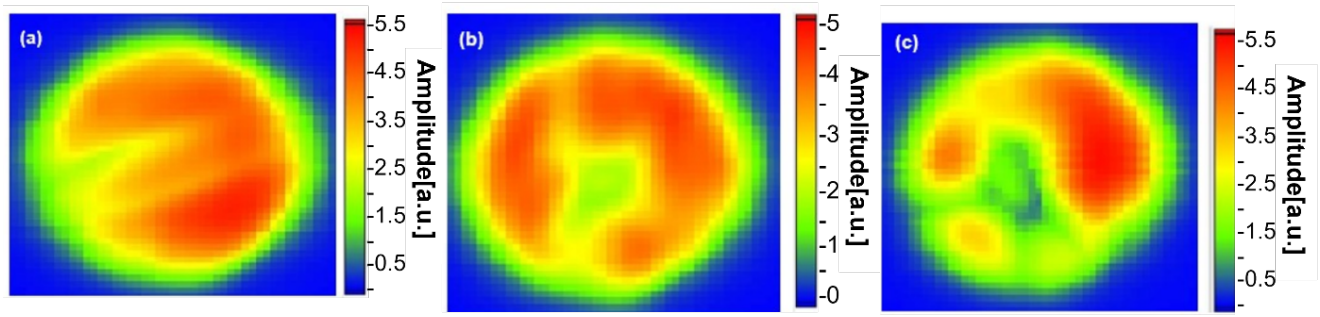

Figure 9: THz absorbance images of the silicone samples: (a) Control sample, (b) Silicone sample with cross-shaped cut, (c) Silicone sample with sponge defect.

The silicone samples were successfully induced with a cross-shaped cut defect and sponge defect. The control sample also sustained scratches during its fabrication. These scratches were clearly seen in the THz images of the control shown in figure 9. The scratches were regions of higher THz absorption in the control. The same behavior was observed for the cross-shaped cut defect as seen in figure 9b. In the images, the mapped THz absorption profiles for both the scratches and the cross-shaped cut were diffused, not showing the actual shape of the defects. This is attributed to the scattering and interferences that happened as the THz was passing through the defects. Although THz imaging was not able to clearly portray the shape of the cut and the scratches, the defects can still be identified because the variations in the images due to higher THz absorption were seen to concentrate in the regions of the defects. Lastly, as seen in figure 9c, the region of the sponge defect was also clearly identifiable in the image, exhibiting higher THz absorption than the silicone.

Plaster of Paris (PoP)

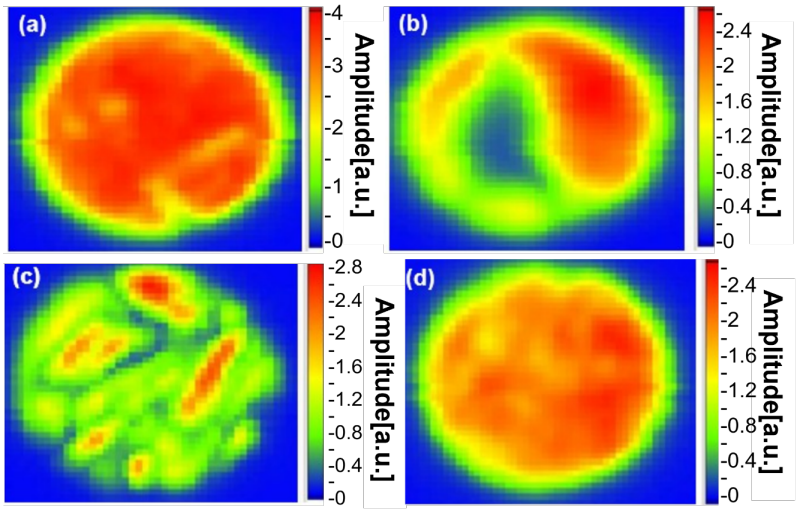

Figure 10: THz absorbance images of the Plaster of Paris samples: (a) Control, (b) PoP with aluminum foil, (c) PoP with styrofoam, and (d) PoP with PET.

The PoP samples were successfully induced with three different defects - aluminum foil, styrofoam, and PET. It can be observed from figure 10 that all the defects have a different THz profile from PoP signifying that THz imaging can be effective in detecting defects. Furthermore, the THz imaging results suggest the possibility of identifying the defect. In figure 10b and 10c, it can be clearly observed that the aluminum foil and styrofoam defects exhibited completely opposite THz responses. The aluminum foil defect has a lower THz transmission profile than the PoP while the styrofoam defect showed higher THz transmission profile than the PoP. Lastly, in figure 10d, the PET defects can be seen as regions of yellow spots scattered throughout the sample. It should be noted that the size of the PET defects is significantly smaller than the other two defects which leads to its distinct THz image profile compared to the other two. This suggests that the defect size can also be predicted in addition to the defect detection in THz imaging. It is important to note that the sample size that can be detected is related to the size of the beam spot which is 0.05 mm. In our experiments, the typical measurable range is from 0.05 - 2 THz. This corresponds to wavelengths of 6 mm to 0.15 mm, respectively. The smallest resolution can range from 3 mm to 0.075 mm within the diffraction limit under conditions where the index of refraction mismatches is relatively small.

Principal Component Analysis

The PCA plots of the samples were successfully generated using the THz absorption coefficient values extracted from the THz images. Figures 11, 12, and 13 show the PCA plots for the PVA, silicone, and PoP samples, respectively. In the analysis, two PCA values are obtained which are labeled PC1 and PC2. From the results, these two PCA values displayed significant clustering for sample differentiation, which is sufficient for phantom defect detection. This resulted from a high contrast of THz amplitudes between the control and defected region. In general, the plots showed clear separation of clusters of samples with defects from the control. This is a good indication that the samples with defects can be distinguished using THz imaging.

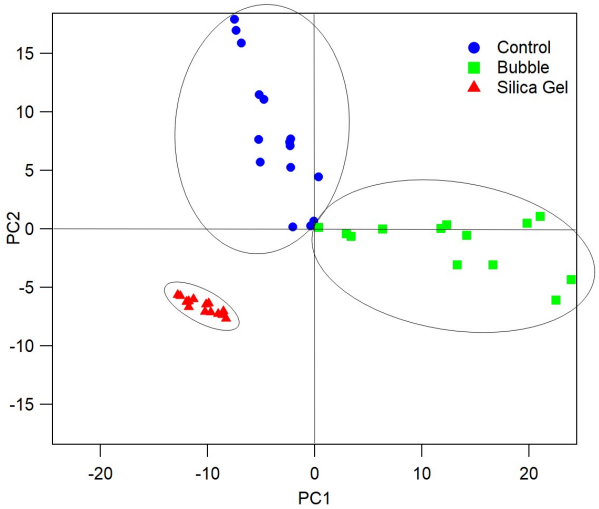

Figure 11: PCA of the PVA samples.

The PCA plot of the PVA samples shown in figure 11 has a PC1 value of 64.7% and a PC2 value of 24.3% with a cumulative variance at 89.0% as shown in figure 11. Three clusters were observed in the plot, which correspond to the three sample conditions. The cluster of the samples with bubble defects was closer to the cluster of the control compared to the cluster of the samples with the silica gel. The silica gel defect cluster also showed higher precision. These suggest that silica gel defects or other defects with similar morphology to silica gel will be easily distinguishable from the control with higher confidence. But, in essence, the PCA plots showed that all the samples can be significantly differentiated from each other using their absorption coefficient values.

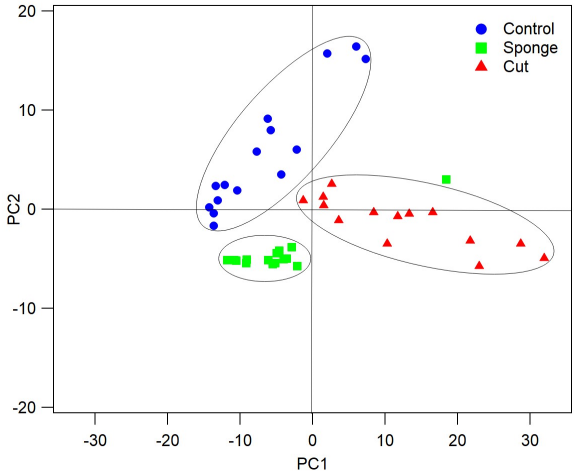

Figure 12: PCA of the silicone samples

The PCA plot of the silicone samples shown in figure 12 has a PC1 value of 67.3% and a PC2 value of 16.1% with a cumulative variance at 83.4%. The clusters of the control and the samples with defects are clearly distinguishable from each other. One data point of the sponge defect cluster is observed to be isolated from the rest and is instead closer to the sample with the cross-shaped cut. This can be attributed to artifacts formed during sample preparation. Regardless, PCA of the silicone samples was able to produce clear distinction between the control silicone sample and the sample with defects.

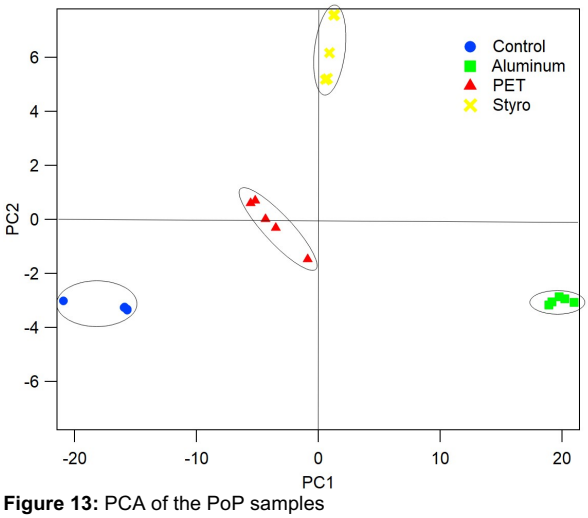

Figure 13: PCA of the PoP samples

Lastly, the PCA of the PoP samples, as shown in figure 13, produced a PC1 value of 86.8% and a PC2 value of 7.7% with a cumulative variance at 94.5%. It can be observed that the clusters are formed far from each other and are clearly distinguishable. In addition, the data points in each cluster are considerably more tightly packed. From these results, it can be concluded that the defects can easily be classified with considerable certainty using PCA of the THz absorption values of the samples.

CONCLUSION AND RECOMMENDATION

The THz images of different phantom-mimicking materials were successfully generated. The THz images revealed that the

samples with defects can be differentiated from the samples without defects owing to the variations in the THz responses of the material and the defects. These results were able to demonstrate the potential of THz imaging for defect characterization and classification in a wide range of phantom-mimicking materials. This was also supported by the PCA results of the samples showing distinct clusters of data points for samples with defects and samples without defects. Further investigation into the enhancement of machine learning techniques for systems with inhomogeneous media, particularly focusing on scenarios involving a larger index of refraction mismatches, to improve the accuracy and generalizability of these approaches is recommended.

ACKNOWLEDGMENT

This work was supported by the Department of Science and Technology-Philippine Council for Industry, Energy, and Emerging Technology Research and Development (DOST-PCIEERD) of the project THz Spectroscopic Fingerprinting of Controlled Substances Relevant to Human Health and Security, under the Terahertz (THz) Research and Innovation Program Leading to Commercially Viable THz Time Domain Spectroscopy Systems.

CONFLICT OF INTEREST

The authors declare no conflict of interest.

CONTRIBUTIONS OF INDIVIDUAL AUTHORS

AG Tapia conceived the original idea of the project. KR Pasoquen, VG Otero, and RS de Ramos wrote the manuscript with assistance from AG Tapia and AC Jusi. AA Salvador and ES Estacio supervised the project. The other authors helped in manufacturing the samples, performing the experiments, and analyzing the data.

REFERENCES

Ali AM, Hogg PJ, England A. European journal of radiology. Eur J Radiol 2018.

Antony A, Mitra J. Analytical chimica acta. Anal Chim Acta 2021;1149:238186.

Berge L, Kaltenecker K, Engelbrecht S, Nguyen A, Skupin S, Merlat L, Fischer B, Zhou B, Thiele I, Jepsen PU. Europhysics letters. Europhys Lett 2019;126(2):24001.

Bowman T, Walter OSNNGMA, El-Shenaweea M. Biomedical physics and engineering express. Biomed Phys Eng Express 2017;3(5).

Brook MA. Biomaterials in plastic surgery. Woodhead Publishing; 2012.

Colditz JC. Journal of hand therapy. J Hand Ther 2002;15(2):144-57.

Dabrowska AK, Rotaru GM, Rossi RM. Skin research and technology. Skin Res Technol 2016;22:3-14.

Di Mauro B, Baccolo G, Garzonio R, Giardino C, Massabo D, Piazzalunga A, Rossini M, Colombo R. The cryosphere. Cryosphere 2017;11:2393-409.

El Haddad J, Bousquet B, Canioni L, Mounaix P. TrAC trends in analytical chemistry. TrAC Trends Anal Chem 2013;44:98-105.

Federici JF, Gary D, Barat R, Michalopoulou ZH. Counterterrorist detection techniques of explosives. Elsevier; 2007:323-66.

Hu J, Xu Z, Li M, He Y, Sun X, Liu Y. Journal of infrared, millimeter, and terahertz waves. J Infrared Millim Terahertz Waves 2021;42:878-92.

Hu J, Zhan C, Shi H, Qiao P, He Y, Liu Y. Infrared physics & technology. Infrared Phys Technol 2023;131:104448.

Jayasanka D, Hernandez-Serrano AI. Investigation of hydrogel skin phantoms using terahertz time-domain spectroscopy. 2022:401-3.

Jiang Y, Ge H, Lian F, Zhang Y, Xia S. RSC advances. RSC Adv 2015;5(114):93979-86.

Jolliffe IT. Philosophical transactions of the royal society A. Philos Trans R Soc A 2016;374(20150202).

Jordens C, Koch M. Optical engineering. Opt Eng 2008;47(3):037003.

Kemp MC. IEEE transactions on terahertz science and technology. IEEE Trans Terahertz Sci Technol 2011;1(1):282-92.

Komikova MR, Cherkasova OP, Nazarov MM, Vrazhnov DA, Kistenev YV, Titov SE, Kopeikina EV, Shevchenko SP, Shkurinov AP. Biomedical optics express. Biomed Opt Express 2021;12(2):1020-35.

Krok P. Quality control of plastic joints with thz-imaging technique. 2014.

LeVier RR, Harrison MC, Lane TH. Journal of clinical epidemiology. J Clin Epidemiol 1995;48(4):513-7.

Li B, Zhao X, Zhang Y, Zhang S, Luo B. Computers and electronics in agriculture. Comput Electron Agric 2020;170:105239.

Mittleman DM. Optics express. Opt Express 2018;26(8):9417-31.

Oh GH, Jeong JH, Park SH, Kim HS. Composites science and technology. Compos Sci Technol 2018;157:67-77.

Riedl AK. Biocomposites: design and mechanical performance. Woodhead Publishing; 2015.

Rostami A, Rasooli H, Baghban H. Terahertz technology: fundamentals and applications. Springer; 2010.

Ruiz Raga S, Qi Y. The journal of physical chemistry C. J Phys Chem C 2016;120.

Sasaki T, Sakamoto T, Otsuka M. Analytical chemistry. Anal Chem 2018;90(3):1677-82.

Shen Y, Yin Y, Li B, Zhao C, Li G. Computers and electronics in agriculture. Comput Electron Agric 2021;181:105931.

Tharwat A. International journal of applied pattern recognition. Int J Appl Pattern Recognit 2016;3(3):197.

Trofimov VA, Varentsova SA, Zakharova IG, Zagursky DY. Sensors. Sensors 2017;17(12):2728.

Wang X, Hu KX, Zhang L, Yu X, Ding EJ. Journal of infrared, millimeter, and terahertz waves. J Infrared Millim Terahertz Waves 2017;38:248-60.

Wang Y, Tai BHY, Shih A. Journal of medical devices. J Med Devices 2014;8(2).

Wegner EG, Krausea D. Procedia CIRP. Procedia CIRP 2023;119:1140-5.

Xie P, Sun Y. Optical and quantum electronics. Opt Quant Electron 2018;50(46).

Yang Y, Dong J, Yue F, Zhang K, Li W. IOP conference series: earth and environmental science. IOP Conf Ser Earth Environ Sci 2021;675(1).

Zhidong C, Lijun Y, Li C, Yuxin H. 2021 46th international conference on infrared, millimeter and terahertz waves (IRMMW-THz). 2021:1-2.